Journal of Organometallic Chemistry, 426 (1992) 369–381
Elsevier Sequoia S.A., Lausanne
JOM 22390

Electron transfer in asymmetric mixed-valence 3,1‴-(propane-1,3-diyl)-1,1′-biferrocenium triiodide

Teng-Yuan Dong
Institute of Chemistry, Academia Sinica, Nankang, Taipei (Taiwan, ROC)

and Hsiu-Mei Lin
Department of Chemistry, National Chung Hsing University, Taichung (Taiwan, ROC)

(Received July 14, 1991)

Abstract

The X-ray structure of 3,1‴-(α-keto-propane-1,3-diyl)-1,1′-biferrocene (**1**) has been determined at 298 K: orthorhombic, $P2_12_12_1$, $a = 7.524(1)$, $b = 10.658(1)$, $c = 22.090(2)$ Å, and $Z = 4$; $D_{calc.} = 1.590$ g cm^{-3}, $R_f = 0.043$, and $R_{wf} = 0.044$. The physical properties of asymmetric mixed-valence 3,1‴-(propane-1,3-diyl)-1,1′-biferrocenium triiodide (**2**) are also reported. The ^{57}Fe Mössbauer and EPR results suggest that compound **2** has a localized electronic structure.

Introduction

The study of intramolecular electron transfer in mixed-valence complexes has enabled systematic and creative investigation into the factors that affect rates of electron transfer in solution redox processes, solid-state materials, and biological electron-transport chains [1–4]. The two most thoroughly studied mixed-valence complexes are the ruthenium amine complexes [4] and the binuclear biferrocenium salts [5]. Mixed-valence trinuclear iron acetate complexes have received attention recently [5]. Furthermore, there have been several studied reported by Gray [6] and others [7–9] where they have begun to examine the distance dependence for biological electron transfer rates. Their general approach has been to attach the $(NH_3)_5Ru^{II}$ moiety to specific histidine imidazoles on metalloproteins.

In the case of mixed-valence biferrocenium salts **3–10** (Scheme 1), considerable progress has been made in understanding the effect of the solid-state environment on the rate of electron transfer [10–13]. For instance, much research effort has

Correspondence to: Dr. T.-Y. Dong, Institute of Chemistry, Academia Sinica, Nankang, Taipei, Taiwan, ROC.

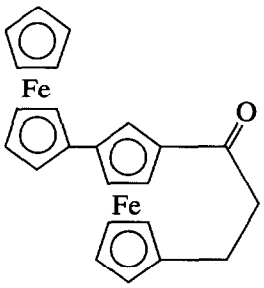

(1)

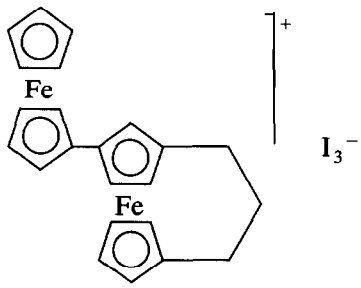

(2)

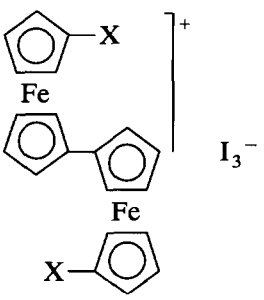

(3) X = H
(4) X = C_2H_5
(5) X = n-C_3H_7
(6) X = n-C_4H_9
(7) X = $CH_2C_6H_5$
(8) X = I
(9) X = Br
(10) X = Cl

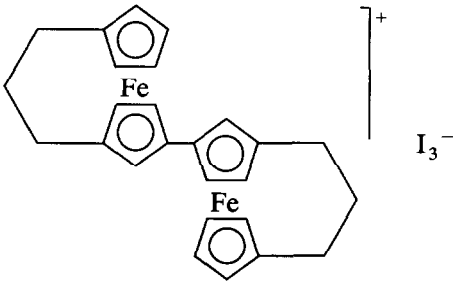

(11)

Scheme 1

addressed the effect of counterions [14,15]. Very recently, it has been found that there is a significant influence on the electron-transfer rate in the mixed-valence biferrocenium salt as the cyclopentadienyl (Cp) rings in each ferrocenyl moiety are linked by an interannular bridge [16]. Such structural modification, *i.e.*, the parallel relation between two Cp rings around the Fe ion, would lead to a larger extent of metal-ligand interactions. In the solid state, compound **11** is judged to have an electron-transfer rate in excess of $\sim 10^{10}$ s^{-1} at 77 K.

In this paper, the results of ^{57}Fe Mössbauer and EPR data for the asymmetric mixed-valence complex **2** are presented in an attempt to understand how the

zero-point energy difference affects the rate of electron transfer. The X-ray single crystal determination of **1** is also reported.

Experimental

General data

As shown in Scheme 2, compounds **1** and **2** were prepared from biferrocene, which was prepared as described in the literature, and identified by melting points, ^{1}H NMR, and mass spectra [17].

Column chromatography was done on neutral alumina (Merck activity I) as the stationary phase. Solvents were purified as follows: ether distilled from Na/benzophenone; CH_2Cl_2 distilled from P_2O_5. All manipulations involving air-sensitive materials were carried out by using standard Schlenk techniques under an atmosphere of N_2.

Acryloylation of biferrocene

The acryloylating reagent was prepared according to the Friedel–Crafts synthesis by mixing acryloyl chloride (0.37 g, 4.1. mmol) and excess $AlCl_3$ in 50 ml of

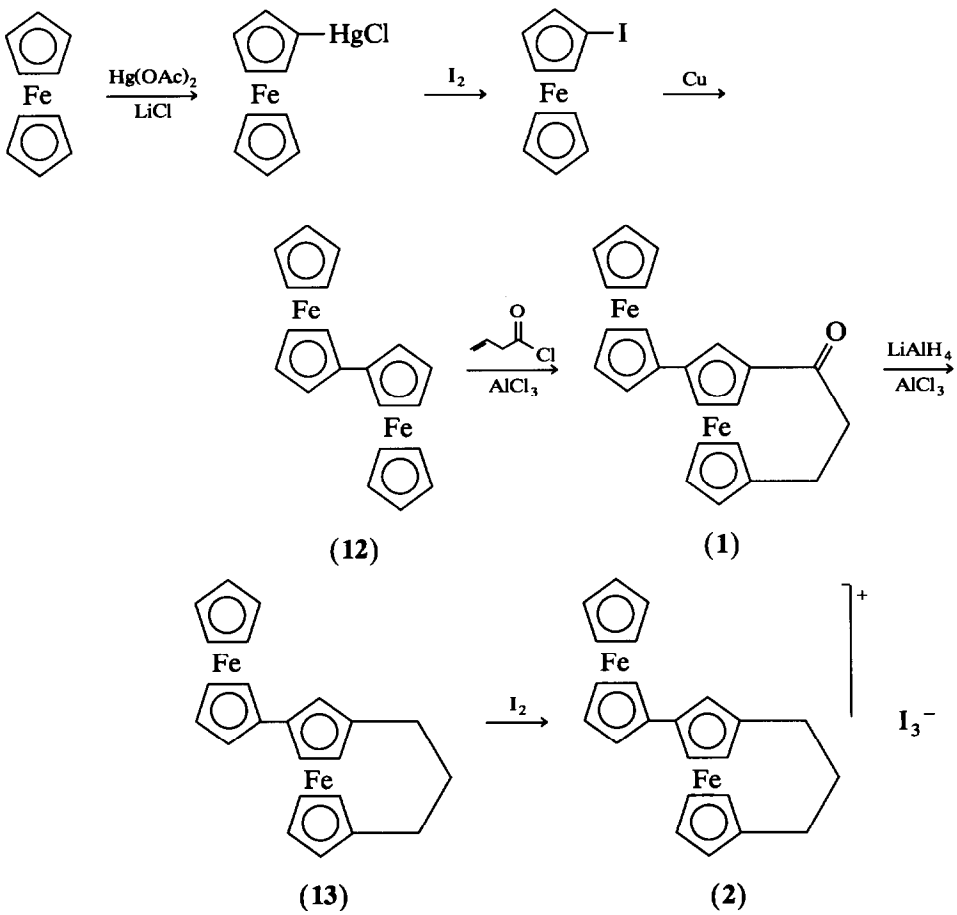

Scheme 2

dried CH_2Cl_2 for 20 min at 0°C under N_2. The excess $AlCl_3$ was filtered out with glass wool.

The acryloylating reagent was added by means of a dropping funnel over a period of about 1 h to a solution of biferrocene (1 g, 2.7 mmol) in 50 ml of dried CH_2Cl_2 at −78°C. The reaction mixture was stirred for 6 h at −78°C. The resulting mixture was separated after the reduction of ferrocenium ion with aqueous $Na_2S_2O_3$. The organic layer was washed with saturated aqueous $NaHCO_3$ and water and it was then dried over $MgSO_4$. The solvent was removed under reduced pressure. The red residue was chromatographed. The first band eluted with hexane was the starting material. The second band eluted with hexane/ether (4:6) was compound **1** (0.34 g, 30%). The crude product was recrystallized from benzene/hexane. The properties of **1** are as follows. ^{1}HNMR ($CDCl_3$, ppm): 2.91 (s, 4H, $-COC_2H_4-$), 3.52 (m, 1H, Cp), 4.05 (s, 5H, Cp), 4.10 (m, 1H, Cp), 4.15–4.18 (m, 2H, Cp), 4.26 (m, 1H, Cp), 4.40 (m, 1H, Cp), 4.45 (m, 1H, Cp), 4.56 (m, 1H, Cp), 4.72 (m, 1H, Cp), 4.84 (m, 1H, Cp), 5.03 (t, 1H, Cp). Mass spectrum: M^+ at m/z 424.

Reduction of 1

The reduction reaction was carried out by carefully adding, with stirring, small portions of $AlCl_3$ to a mixture of **1** and $LiAlH_4$ in dried ether. After 40 min, the solution became yellow, an excess of H_2O was added to it, and the ether layer was separated. The ether layer was washed with water and dried over $MgSO_4$. After the evaporation of the solvent, the crude product was chromatographed using hexane as the eluting solvent and recrystallized from benzene/hexane in a yield of approximately 90%. The physical properties of **13** are as follows: m.p. 187–188°C. ^{1}H NMR ($CDCl_3$, ppm): 1.96 (s, 6H, $-C_3H_6-$), 3.52 (s, 1H, Cp), 3.83 (s, 1H, Cp), 3.96 (s, 1H, Cp), 4.08 (s, 5H, Cp), 4.10–4.12 (m, 4H, Cp), 4.19 (m, 3H, Cp), 4.29 (t, 1H, Cp). Mass spectrum: M^+ at m/z 410.

Mixed-valence compound

Compound **2** was prepared according to the simple procedure previously reported for biferrocenium triiodide [18]. Anal. Found: C, 35.46; H, 2.73. $C_{23}H_{22}Fe_2I_3$ calc.: C, 34.93; H, 2.98%.

Physical methods

The ^{57}Fe Mössbauer spectra were run on a constant-acceleration instrument which has been previously described [15]. We estimate the absolute temperature accuracy to be ±1 K. Velocity calibrations were made using a 99.99% pure 10 μm iron foil. Typical line widths for all three pairs of iron lines fell in the range 0.28–0.30 mm s^{-1}. The isomer shifts are given relative to iron foil at 300 K with no second-order Doppler effects.

^{1}H NMR spectra were run on a Bruker MSL 200 spectrometer. Mass spectra were obtained with a VG system, model 70-250 S. Electron paramagnetic resonance data (X-band) were collected with a Bruker ER200D-SRC spectrometer. The magnetic field was calibrated with a Bruker ER035M NMR gauss meter. DPPH was used to gauge the microwave frequency. A direct-immersion Dewar, which was inserted into the cavity, was used to obtain the data at 77 K.

Table 1

Experimental and crystal data for the X-ray structure of **1**

Chemical formula	$C_{23}H_{20}Fe_2O$
Crystal system	Orthorhombic
Space group	$P2_12_12_1$
a (Å)	7.524(1)
b (Å)	10.658(1)
c (Å)	22.090(2)
V (Å^3)	1771.35
Z	4
Formula weight (g mol^{-1})	423.96
$\rho_{calc.}$ (g mol^{-1})	1.590
μ (mm^{-1})	1.65
λ (Å)	0.70930
2θ (max)	44.8
Trans. coeff. (max, min)	1.000, 0.971
R_f	0.043
R_{wf}	0.044

Structure of determination of 1

A block crystal (0.25–0.08–0.12 mm^3), which was grown by slowly evaporating the hexane solution of **1**, was used for data collection at room temperature. Cell dimensions and space group data were determined by standard methods on an Enraf–Nonius CAD4 diffractometer. The θ–2θ scan technique was used to record the intensities for all nonequivalent reflects for which $1° < 2\theta < 44.8°$. Absorption corrections were made. Of the 1354 independent intensities, there are 839 with $F_o > 2.5\sigma(F_o^2)$, where $\sigma(F_o^2)$ was estimated from counting statistics. These data were used in the final refinement of the structural parameters. The X-ray crystal data are summarized in Table 1.

A three-dimensional Patterson synthesis was used to determine heavy-atom positions, which phased the data sufficiently well to permit location of the remaining non-hydrogen atoms from Fourier synthesis. All nonhydrogen atoms were refined anisotropically. During the final cycles of refinement, fixed hydrogen contributions with C–H bond lengths fixed at 1.08 Å were applied. The final positional parameters for all atoms are given in Table 2, and the selected bond distances and angles are given in Table 3. Listings of the thermal parameters and observed and calculated structure factors are given in the supplementary material.

Results and discussion

Methodology

Compound **13** was previously prepared by cross-coupling ferrocenylzinc chloride with 3-iodo-1,1′-(propane-1,3-diyl)ferrocene using dichloro[1,1′-bis(diphenylphosphine)ferrocene]palladium(II) as a catalyst (Scheme 3) [19]. In comparison with the cross-coupling reaction, our preparation is much more convenient in terms of yield and economy. The cross-coupling reaction involves more steps and highly air-sensitive materials. Furthermore, our structural determination of **1** has given insight

Table 2

Atomic coordinates and thermal parameters for **1**

Atom	x	y	z	B_{iso}
Fe1	0.06597(24)	0.98687(15)	0.00426(8)	3.34(8)
Fe2	−0.31054(26)	0.94705(18)	0.19577(9)	3.96(9)
O	−0.0806(19)	1.1138(12)	0.3280(5)	10.3(8)
C1	−0.1184(15)	0.9344(11)	0.0665(5)	3.2(6)
C2	−0.1970(17)	0.9690(11)	0.0127(5)	4.3(6)
C3	−0.1420(18)	0.8923(12)	−0.0348(6)	4.5(7)
C4	−0.0168(19)	0.8086(11)	−0.0089(7)	5.2(8)
C5	−0.0034(17)	0.8319(11)	0.0528(5)	3.7(7)
C6	0.1903(25)	1.1391(16)	0.0373(7)	7.7(10)
C7	0.1196(18)	1.1683(13)	−0.0152(8)	7.1(10)
C8	0.1942(21)	1.0877(14)	−0.0598(6)	6.0(8)
C9	0.3132(17)	1.0099(12)	−0.0307(6)	5.4(8)
C10	0.3137(20)	1.0423(14)	0.0300(6)	6.3(8)
C11	−0.1351(16)	0.9905(12)	0.1260(5)	3.9(6)
C12	−0.0489(15)	0.9564(10)	0.1818(5)	3.3(6)
C13	−0.1067(17)	1.0392(12)	0.2287(6)	4.6(7)
C14	−0.2241(18)	1.1270(10)	0.2012(6)	4.5(7)
C15	−0.2510(20)	1.0957(12)	0.1404(6)	5.3(7)
C16	−0.4645(23)	0.8018(17)	0.1749(7)	8.0(10)
C17	−0.3515(21)	0.7689(14)	0.2193(6)	5.6(8)
C18	−0.3810(18)	0.8440(13)	0.2684(6)	4.7(7)
C19	−0.5168(21)	0.9232(15)	0.2522(8)	7.6(10)
C20	−0.5678(21)	0.8935(23)	0.1950(8)	12.9(15)
C21	−0.0833(19)	1.0231(14)	0.2941(6)	5.8(8)
C22	−0.0823(26)	0.8931(16)	0.3174(8)	8.6(11)
C23	−0.2748(26)	0.8486(18)	0.3260(7)	9.0(12)
H2	−0.294	1.036	0.007	6.3
H3	−0.183	0.905	−0.078	6.3
H4	0.042	0.775	−0.023	6.3
H5	0.064	0.782	0.083	6.3
H6	0.194	1.127	0.085	6.3
H7	0.026	1.194	−0.047	6.3
H8	0.206	1.120	−0.103	6.3
H9	0.403	0.946	−0.042	6.3
H10	0.392	0.980	0.053	6.3
H12	0.048	0.891	0.187	6.3
H14	−0.234	1.189	0.233	6.3
H15	−0.338	1.151	0.117	6.3
H16	−0.466	0.796	0.130	6.3
H17	−0.271	0.693	0.216	6.3
H19	−0.603	0.984	0.274	6.3
H20	−0.661	0.909	0.164	6.3
H22-1	−0.054	0.910	0.363	6.3
H22-2	−0.021	0.828	0.296	6.3
H23-1	−0.335	0.783	0.352	6.3
H23-2	−0.331	0.931	0.345	6.3

into the mechanism of acryloylation of biferrocene. In the case of acryloylation of ferrocene, Watts reported that the attacking species is the acyl cation, either free or as an ion pair [20]. It has also been reported that the free Cp ring is more

Table 3

Selected bond distances (Å) and angles (deg) for **1**

Fe(1)–C(1)	2.03(1)	C(2)–C(3)	1.39(2)
Fe(1)–C(2)	2.00(1)	C(3)–C(4)	1.42(2)
Fe(1)–C(3)	2.05(1)	C(4)–C(5)	1.39(2)
Fe(1)–C(4)	2.02(1)	C(6)–C(7)	1.31(2)
Fe(1)–C(5)	2.04(1)	C(6)–C(10)	1.40(2)
Fe(1)–C(6)	2.01(2)	C(7)–C(8)	1.42(2)
Fe(1)–C(7)	2.02(1)	C(8)–C(9)	1.38(2)
Fe(1)–C(8)	2.02(1)	C(9)–C(10)	1.38(2)
Fe(1)–C(9)	2.03(1)	C(11)–C(12)	1.44(2)
Fe(1)–C(10)	2.04(2)	C(11)–C(15)	1.46(2)
Fe(2)–C(11)	2.08(1)	C(12)–C(13)	1.43(2)
Fe(2)–C(12)	2.00(1)	C(13)–C(14)	1.42(2)
Fe(2)–C(13)	1.96(1)	C(13)–C(21)	1.47(2)
Fe(2)–C(14)	2.03(1)	C(14)–C(15)	1.40(2)
Fe(2)–C(15)	2.05(1)	C(16)–C(17)	1.34(2)
Fe(2)–C(16)	1.99(2)	C(16)–C(20)	1.33(3)
Fe(2)–C(17)	1.99(1)	C(17)–C(18)	1.37(2)
Fe(2)–C(18)	2.02(1)	C(18)–C(19)	1.37(2)
Fe(2)–C(19)	2.01(2)	C(18)–C(23)	1.50(2)
Fe(20)–C(20)	2.02(2)	C(19)–C(20)	1.36(3)
C(1)–C(2)	1.38(2)	C(21)–C(22)	1.48(2)
C(1)–C(5)	1.45(2)	C(22)–C(23)	1.54(3)
C(1)–C(11)	1.45(2)		
C(2)–C(1)–C(5)	106.4(2)	C(12)–C(13)–C(21)	127.3(1)
C(2)–C(1)–C(11)	129.4(1)	C(14)–C(13)–C(21)	124.9(1)
C(5)–C(1)–C(11)	124.1(1)	C(13)–C(14)–C(15)	110.0(1)
C(1)–C(2)–C(3)	111.4(1)	C(11)–C(15)–C(14)	107.8(1)
C(1)–C(5)–C(4)	107.5(1)	C(16)–C(17)–C(18)	108.8(1)
C(7)–C(6)–C(10)	110.2(1)	C(17)–C(18)–C(19)	105.9(1)
C(6)–C(7)–C(8)	108.0(1)	C(17)–C(18)–C(23)	127.2(1)
C(7)–C(8)–C(9)	107.1(1)	C(19)–C(18)–C(23)	126.6(2)
C(8)–C(9)–C(10)	107.7(1)	C(18)–C(19)–C(20)	108.0(2)
C(6)–C(10)–C(9)	107.1(1)	C(16)–C(20)–C(19)	108.6(2)
C(1)–C(11)–C(12)	129.3(1)	O–C(21)–C(13)	120.9(1)
C(1)–C(11)–C(15)	124.5(1)	O–C(21)–C(22)	121.8(1)
C(12)–C(11)–C(15)	106.2(1)	C(13)–C(21)–C(22)	117.0(1)
C(11)–C(12)–C(13)	109.1(1)	C(21)–C(22)–C(23)	109.1(1)
C(12)–C(13)–C(14)	106.6(1)	C(18)–C(23)–C(22)	114.0(1)

reactive than the fulvalenide (Scheme 4) [15]. If the above suggestions are correct, then the product would be compound **14** in the acryloylation of biferrocene. However, we find that the product is compound **1** instead of **14**. Hence, we propose that the attacking species of acryloylation of biferrocene at −78°C is cation **15** as shown in Scheme 4.

Molecular structure of 1

The results of our crystallographic study of **1** show that it crystallizes in the orthorhombic space group $P2_12_12_1$. Figure 1 shows the molecular structure and atomic labelling scheme. Atomic coordinates and selected bond distances and angles are shown in Tables 2 and 3. As shown in Fig. 1, the Cp rings associated

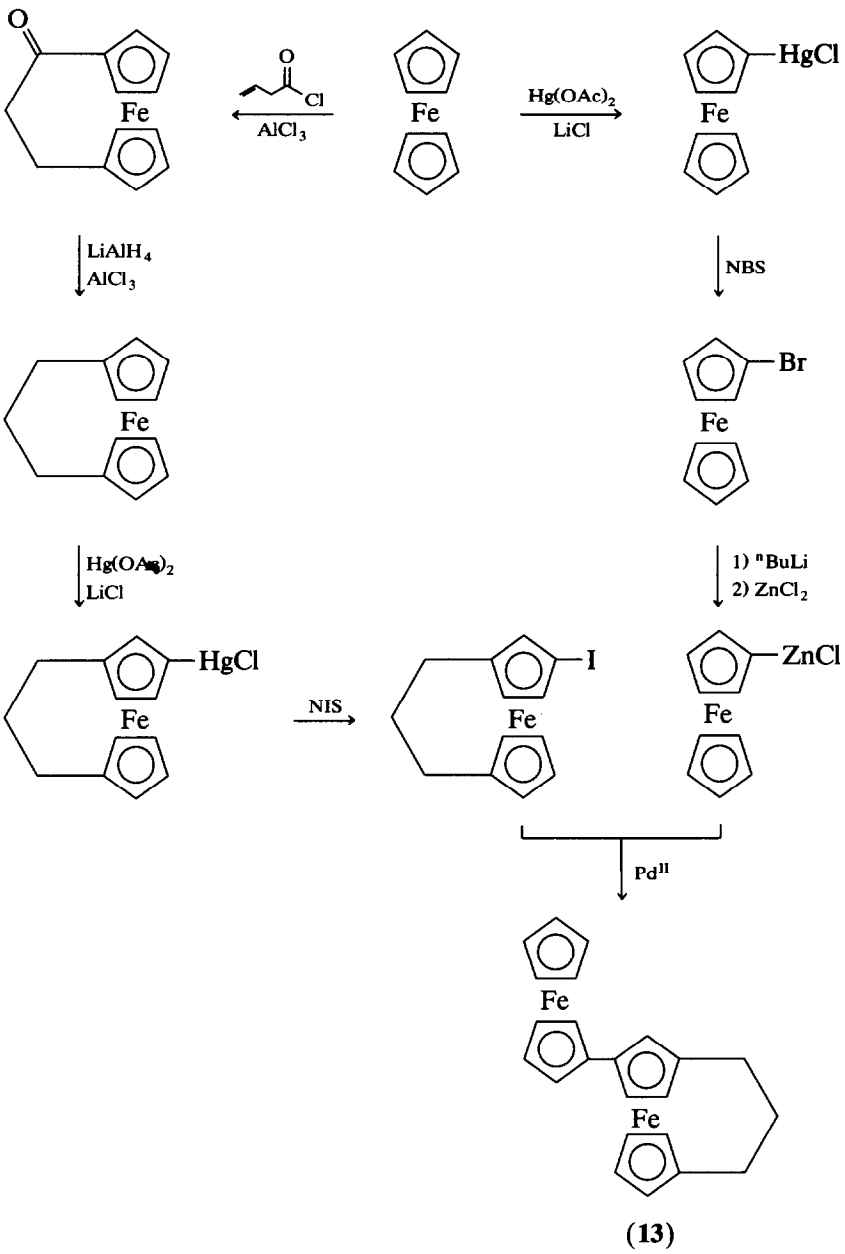

(13)

Scheme 3

with Fe1 are not perfectly eclipsed, but are rotated relative to one another by 6.2°. The Fe–C distances range from 1.996 to 2.036 Å. The spread of distances is due to the nonparallel Cp rings where the angle between the two least-squares rings is 2.2°. The average of these Fe–C distances, *i.e.*, 2.0254 Å, is smaller than 2.045 Å observed for ferrocene [21]. Furthermore, the average of the distances (1.649 and 1.641 Å) between Fe and the centre of mass of the ring is 1.645 Å which compares

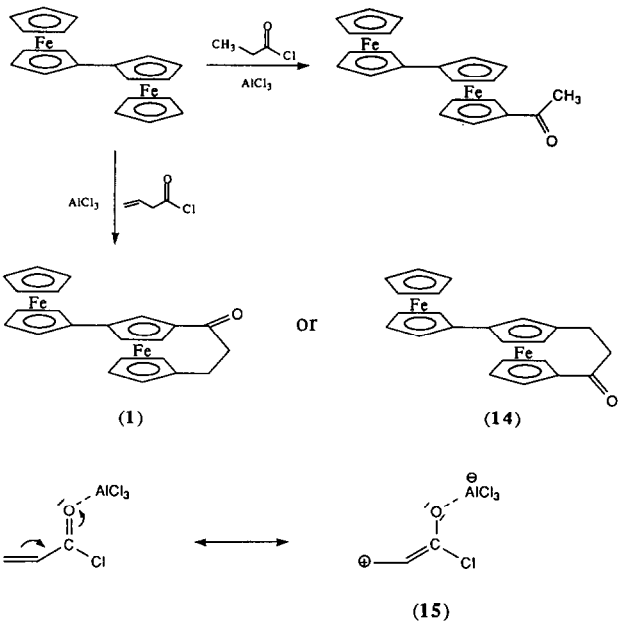

Scheme 4

well with ferrocene (1.65 Å) [21]. In the case of Cp associated with Fe2, the dihedral angle between the two least-squares Cp rings is 9.4° which is even larger than the value of 8.8° in α-keto-1,1′-trimethyleneferrocene [22]. Owing to the nonparallel Cp rings, the Fe–C distances spread from 1.961 to 2.081 Å and the

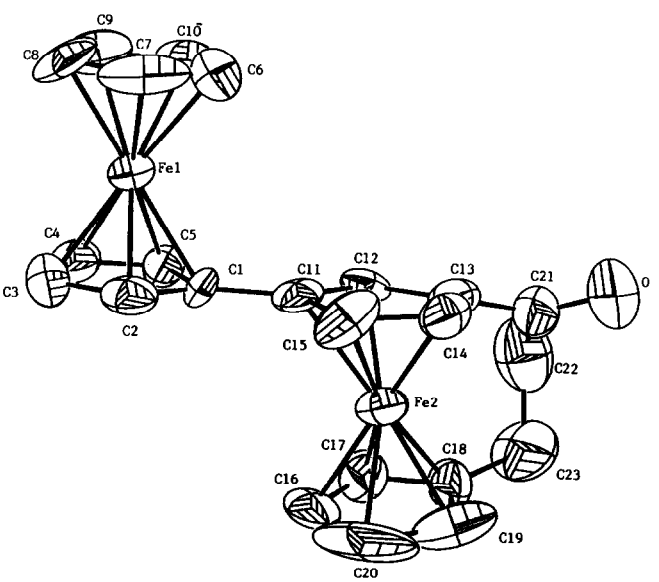

Fig. 1. ORTEP plot of molecule of 1.

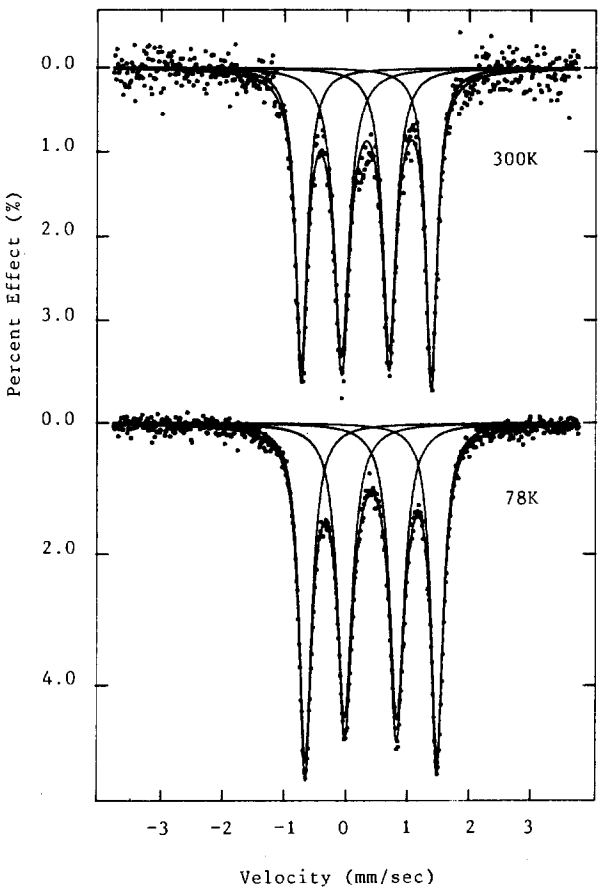

Fig. 2. ^{57}Fe Mössbauer spectra of **2**.

average value (2.014Å) is smaller than that in ferrocene (2.045 Å). The two Cp rings are also not perfectly eclipsed (6.2°). Inspection of the iron to the centre of mass of Cp ring bond lengths shows that both distances (1.617 and 1.639 Å) are smaller than the value of 1.65 Å in ferrocene. From this comparison, we can conclude that the interannular α-keto-trimethylene bridge squeezes the Fe atom.

^{57}Fe Mössbauer characteristics of 2

As shown in Fig. 2, the 300 and 77 K Mössbauer spectra of **2** were obtained, and the absorption peaks were least-squares fitted to Lorentzian lines. The resulting fitting parameters are collected in Table 4. The features in the 77 K Mössbauer spectra of **2** are two doublets, one for Fe^{II} metallocene ($\Delta E_Q = 2.137$ mm s^{-1}) and the other for Fe^{III} metallocene ($\Delta E_Q = 0.841$ mm s^{-1}). This pattern of two doublets is what is expected for a mixed-valence biferrocenium salt that is valence trapped on the time scale of the Mössbauer technique (electron-transfer rate less than $\sim 10^{10}$ s^{-1}). It has been reported that the most important factor controlling the intramolecular electron transfer in a mixed-valence biferrocenium salt is the symmetry of the cation [15]. The cation in **2** is not symmetric; that is, the two irons

Table 4

^{57}Fe Mössbauer least-squares fitting parameters of **2**

T(K)	ΔE_Q [a]	δ [b]	Γ [c]
300	0.771	0.418	0.265, 0.295
	2.111	0.434	0.225, 0.229
77	0.841	0.514	0.284, 0.291
	2.137	0.521	0.239, 0.245

[a] Quadrupole splitting. [b] Isomer shift. [c] Full width at half height taken from the least-squares fitting program. The width for the line at more positive velocity is listed first for each doublet.

are not in equivalent environments. This asymmetry induces a nonzero zero-point energy barrier for intramolecular electron transfer. One vibronic state of the mixed-valence cation, *i.e.*, $Fe_a^{II}Fe_b^{III}$, is energetically more stable than the other state, $Fe_b^{II}Fe_a^{III}$. This explains why a localized electronic structure in **2** and a delocalized electronic structure in **11** were observed. As the temperature of the sample is increased to 300 K, it is interesting to find that the two doublets do not move together. In fact, the values of ΔE_Q for these two doublets at 300 K Mössbauer spectrum are smaller than those in the 77K spectrum. In comparison with mixed-valence cation **3**, we also find that the value of ΔE_Q in the ferrocenium doublet is unusually large [10]. In the case of **3**, the ΔE_Q for the ferrocenium doublet is about 0.4 mm s^{-1} [10]. In general, the decrease of ΔE_Q in the ferrocenyl doublet and the increase of ΔE_Q in the ferrocenium doublet are related to the degree of intramolecular electron transfer in the mixed-valence biferrocenium cation. In other words, the rate of electron transfer in **2** is faster than **3**.

Electron paramagnetic resonance

For a mononuclear ferrocenium cation with no low-symmetry crystal field distortion, an axial-type spectrum will be observed with $g_\parallel = 6$ and $g_\perp = 0$ [23]. As the low-symmetry crystal field increases, both $g_\parallel$ and $g_\perp$ approach a value of 2. In the case of binuclear mixed-valence biferrocenium cation, the value of g tensor anisotropy ($\Delta g = g_\parallel - g_\perp$) is considerably reduced. Hendrickson suggested that this is a reflection of considerably reduced orbital angular momentum in the ground state that results from admixture of the $S = 0$ Fe^{II} description into the ground state [11].

The powder X-band EPR spectra for **2** obtained at 77 and 300 K are shown in Fig. 3. The g values evaluated from these spectra and other related EPR spectra are collected in Table 5. There are several features in the $g_\parallel$ region for the 77 K EPR spectrum of **2**. We believe that this is owing to the anisotropic crystallization of the sample. Therefore, the 77 K EPR spectrum was taken in frozen ethanol solution. A typical axial-type EPR spectrum was observed in frozen ethanol solution ($g_\parallel = 3.06$ and $g_\perp = 1.93$). The Δg value is 1.13 which is smaller than 1.93 observed for biferrocenium triiodide [11]. The origin of the reduced Δg value is that the cation of **2** can experience a greater low-symmetry crystal field than the biferrocenium cation. Furthermore, as found in 1,1'-(propane-1,3-diyl)ferrocenium cation, the 300 K powder EPR spectrum of **2** can also be observed [16]. The electronic ground state for ferrocenium cation is a doublet, $^2E_{2g}$ ($a_{1g}{}^2e_{2g}{}^3$), and

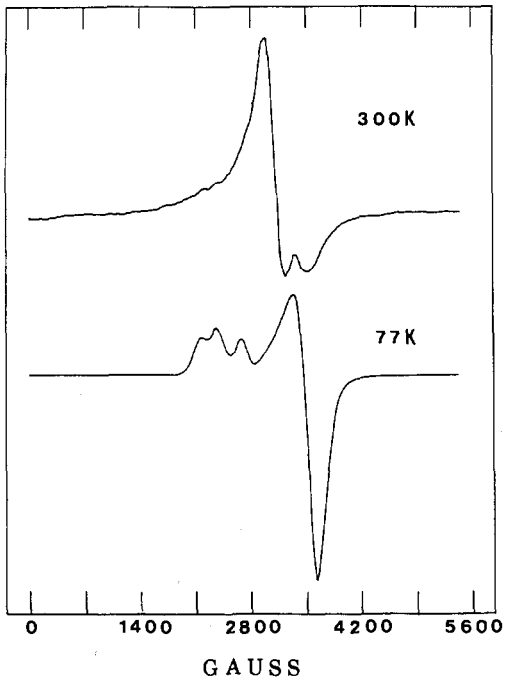

Fig. 3. Powder X-band EPR spectra of **2**.

EPR signals can generally only be seen at low temperatures as a result of fast spin lattice relaxation. Very recently, we found that the interannular bridge in 1,1'-(propane-1,3-diyl)ferrocenium can tilt the Cp rings from the parallel geometry for ferrocenium [16]. Bending back the Cp rings splits the e_{2g} set into orbitals of a_1 ($d_{x^2-y^2}$) and b_2 (d_{xy}) symmetry. We proposed that the splitting of e_{2g} orbitals is the origin of the EPR signals which can be seen at room temperature. This is also the case in **2**.

The EPR studies of **2** can also provide us with the important fact that the rate of electron transfer in **11** is greater than the EPR time scale ($\sim 10^{10}$ s^{-1}). In general, if the Δg value for a given mixed-valence biferrocenium cation is smaller than 0.75, then the rate of electron transfer is greater than the EPR time scale. In

Table 5

EPR data for **2** and **11**

Compound	T(K)	$g_{\parallel}$	$g_{\perp}$	Δg [a]
2	300	1.92	2.17	
	77	3.14 [b]	1.97	1.17
	77 [c]	3.06	1.93	1.13
11	300	2.00		
	77	2.71	1.98	0.73

[a] $\Delta g = g_{\parallel} - g_{\perp}$. [b] Two signals can be also observed at $g_{\parallel} = 2.88$ and 2.56. [c] In frozen C_2H_5OH solution.

the case of **11**, the admixture of the $S = 0$ Fe^{II} description into the ground state of ferrocenium and the low-symmetry crystal field distortion can contribute to a smaller g tensor anisotropy (Δg). The Δg value is 0.73 for **11**. From our EPR studies, we can conclude that the considerably reduced Δg value in **11** is attributed to the greater admixture of the $S = 0$ Fe^{II} description. Since the cation of **2** could experience a greater low-symmetry crystal field than that in the cation of **11**. In other words, if the smaller Δg value in **11** is only attributed to the low-symmetry crystal field, then the Δg value has to be greater than 1.13.

Conclusion

Our structural determination of **1** has given insight about the mechanism of acryloylation of biferrocene. From our Mössbauer and EPR studies, compound **2** has a localized electronic structure. However, compound **11** has a delocalized electronic structure on the EPR time scale.

Supplementary material available. Tables of thermal parameters (1 page) and structure factors (5 pages) are available from the authors.

Acknowledgement

We are grateful for support from the ROC National Science Council.

References

1 P. Day, Int. Rev. Phys. Chem., 1 (1981) 149.
2 D. Brown (Ed.), Mixed-Valence Compounds, Theory and Applications in Chemistry, Physics, Geology and Biology, Riedel, Boston, MA, 1980.
3 C. Creutz, Prog. Inorg. Chem., 30 (1983) 1.
4 D.E. Richardson and H. Taube, Coord. Chem. Rev., 60 (1984) 107.
5 D.N. Hendrickson, S.M. Oh, T.-Y. Dong, T. Kambara, M.J. Cohn and M.F. Moore, Comments Inorg. Chem., 4 (1985) 329.
6 M.J. Therien, M. Selman and H.B. Gray, J. Am. Chem. Soc., 112 (1990) 2420.
7 A. Vassilian, J.F. Wishart, B. Hemelryck, H. Schwarz and S.S. Isied, J. Am. Chem. Soc., 112 (1990) 7278.
8 M.R. DeFelippis, M. Faraggi and M.H. Klapper, J. Am. Chem. Soc., 112 (1990) 5640.
9 N.S. Hush, M.N. Paddon-Row, E. Cotsaris, H. Oevering, J.W. Verhoeven and M. Heppener, Chem. Phys. Lett., 17 (1985) 8.
10 T.-Y. Dong, D.N. Hendrickson, K. Iwai, M.J. Cohn, S.J. Geib, A.L. Rheingold, H. Sano, I. Motoyama and S. Nakashima, J. Am. Chem. Soc., 107 (1985) 7996.
11 T.-Y. Dong, D.N. Hendrickson, C.G. Pierpont and M.F. Moore, J. Am. Chem. Soc., 108 (1986) 963.
12 S. Iijima, R. Saida, I. Motoyama and H. Sano, Bull. Chem. Soc. Jpn., 54 (1981) 1375.
13 S. Nakashima, M. Katada, I. Motoyama and H. Sano, Bull. Chem. Sóc. Jpn., 60 (1987) 2253.
14 M. Kai, M. Katada and H. Sano, Chem. Lett., (1988) 1523.
15 T.-Y. Dong, C.C. Schei, T.L. Hsu, S.L. Lee and S.J. Li, Inorg. Chem., 30 (1991) 2457.
16 T.-Y. Dong and C.Y. Chou, J. Chem. Soc., Chem. Commun., (1990) 1332.
17 M.D. Rausch, J. Org. Chem., 26 (1961) 1802.
18 W.H. Jr. Morrison and D.N. Hendrickson, Inorg. Chem., 14 (1975) 2331.
19 D.R. Talham and D.O. Cowan, Organometallics, 6 (1987) 932.
20 T.D. Turbitt and W.E. Watts, J. Organomet. Chem., 46 (1972) 109.
21 P. Seiler and J.D. Dunitz, Acta Crystallogr., Sect. B, 28 (1972) 1331.
22 N.D. Janes, R.E. Marsh and J.H. Richards, Acta Crystallogr., 19 (1965) 330.
23 R. Prins, Mol. Phys., 19 (1970) 603.